Journal of Alloys and Compounds 506 (2010) 772–776

Contents lists available at ScienceDirect

Journal of Alloys and Compounds

journal homepage: www.elsevier.com/locate/jallcom

Effect of Al doping on the visible photoluminescence of ZnO nanofibers

Yanxia Liu, Hongliang Zhang, Xiuyun An, Caitian Gao, Zhenxing Zhang, Jinyuan Zhou, Ming Zhou, Erqing Xie*

Key Laboratory for Magnetism and Magnetic Materials of the Ministry of Education, Lanzhou University, Lanzhou 730000, Gansu, People's Republic of China

ARTICLE INFO

Article history:
Received 6 June 2010
Received in revised form 2 July 2010
Accepted 7 July 2010
Available online 15 July 2010

Keywords:
ZnO nanofibers
Al doping
Electrospinning
Photoluminescence

ABSTRACT

ZnO nanofibers doped with different Al concentration were fabricated by electrospinning method. The nanofibers annealed at 600 °C showed a polycrystalline hexagonal structure with the diameter of about 150 nm. The grain size of the nanofibers decreased after Al doping. The photoluminescence spectra of all the samples presented two luminescence bands at green and orange ranges. And both bands decreased simultaneously with the Al concentration increasing. The luminescence centers of the green and orange bands could be attributed to oxygen vacancies and excess oxygen, which might reside inside the polycrystalline grains and near the grain boundaries, respectively. And the simultaneous decrease of both luminescence bands in the Al-doped ZnO nanofibers might be due to the inwards penetration of excess oxygen.

1. Introduction

One-dimensional ZnO nanomaterials have attracted great attentions due to their fascinating properties. During the recent years, much effort has been devoted to synthesize ZnO nanomaterials through various approaches [1–6]. Among them, electrospinning technique is a versatile and economical approach. The electrospun ZnO nanofibers are long in length, uniform in diameter, and diverse in composition [7–9]. As a wide band-gap semiconductor, ZnO nanomaterials should also be considered as a promising candidate to be used as the host materials for doping other elements. Numbers of studies have pointed out that the doped ZnO nanomaterials showed enhanced and controllable electrical, optical, and magnetical performances [10–12]. In particular, Al-doped ZnO nanomaterials, which have shown competitive properties as indium tin oxide and with much lower fabrication cost, have triggered tremendous motivation because of their potential applications as transparent conductive oxide material [13]. Thus investigations on optical properties, including photoluminescence (PL) property, of Al-doped ZnO nanomaterials are of great importance.

On the other hand, PL spectroscopy has been widely used to characterize the defects and impurities in the materials. Generally, three luminescence bands in the ultraviolet (UV), green, and yellow–orange ranges can be observed from both undoped and Al-doped ZnO [11,14]. And, it is well understood that UV emission at about 380 nm is derived from near-band-gap emission (NBE) of ZnO. However, the origins of the luminescences in the visible range are still in controversy. Several models have been established to explain these luminescence bands [15–18]. Djurisic et al. have observed that the green emission shown a direct correlation with the surface hydroxide concentrations, and suggested that the green luminescence of ZnO nanostructures should be attributed to the surface centers [15,16,19]. Whereas several researchers have reported that the green luminescence in ZnO could be assigned to the oxygen vacancies related defects [17,20,21]. Besides, the origin of yellow–orange luminescence band has not been completely understood either, most studies were mainly focused on the excess oxygen [18,22,23] and OH groups on the surface [24,25]. Therefore, it is still of great interests in further investigating the origins of the green and yellow–orange luminescences of ZnO nanomaterials.

In the present work, undoped and Al-doped ZnO nanofibers were fabricated by electrospinning technique. The dependence of PL spectra on the Al doping has been mainly explored. And the origins of the green and orange luminescence bands have also been discussed.

2. Experimental

Al-doped ZnO nanofibers were prepared by electrospinning technique with a sol–gel aqueous solution. First, the sol–gel aqueous solutions were prepared by dissolving zinc acetate dihydrate ($Zn(CH_3COO)_2{\cdot}2H_2O$), aluminum nitrate nanohydrate ($Al(NO_3)_3{\cdot}9H_2O$), and PVA powder (10 wt%) in deionized water. Zinc acetate and aluminum nitrate were used as precursor and doping source, respectively. The mole ratio of Al/(Zn + Al) ranged from 0 to 5%, respectively. Then the solutions were heated at 60 °C under a vigorous magnetic stirring to yield clear and homogeneous solutions. After stirring for 6 h, the solutions were injected into an electrospinning apparatus, which was assembled with a glass syringe, a stainless needle with the inner diam-

* Corresponding author. Tel.: +86 931 8912616; fax: +86 931 8913554.
E-mail address: xieeq@lzu.edu.cn (E. Xie).

0925-8388/$ – see front matter © 2010 Elsevier B.V. All rights reserved.
doi:10.1016/j.jallcom.2010.07.067

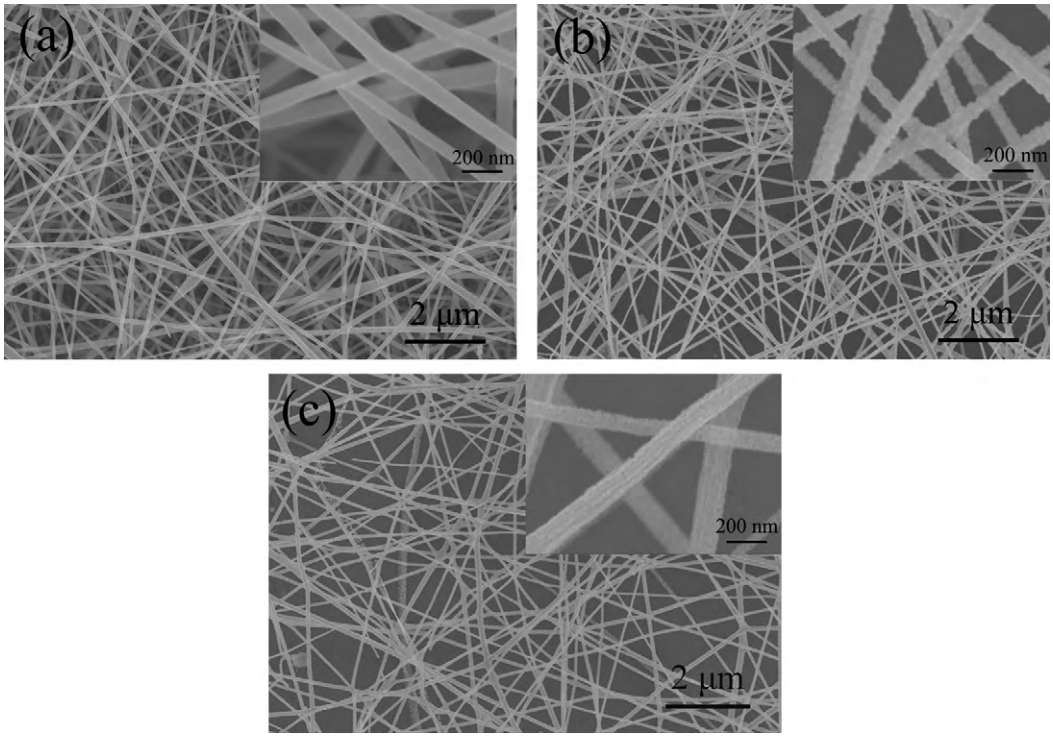

Fig. 1. SEM images of the as-spun ZnO with PVA (a), the obtained undoped ZnO (b), and 5% Al-doped ZnO (c) nanofibers after annealing at 600 °C in O_2. The insets show their corresponding enlarged images.

eter of about 0.5 mm, a DC high-voltage source, and a grounded iron sheet as the collector of nanofibers. During the electrospinning process, the distance and the voltage between the needle and the iron sheet were 15 cm and 18 kV, respectively. And the spun nanofibers were collected on the n-type (1 1 1) silicon substrates in air for further treatments. Finally, the as-spun nanofibers collected on the silicon substrates were annealed in O_2 or air ambient at 600 °C for 2 h to decompose PVA and obtain undoped or Al-doped ZnO nanofibers.

The morphologies of the samples were observed by FE-SEM (Hitachi S-4800) at an accelerating voltage of 5 kV. XRD spectra of the samples were conducted on a Philips X'pert Pro X-ray diffractometer equipped with a CuK_α source ($\lambda = 0.15406$ nm) at an incident angle of 1°. Micro-Raman spectra of the samples were recorded on a JY-HR800 micro-Raman spectrometer using a 532 nm wavelength YAG laser. The PL properties of the ZnO nanofibers were measured on a spectrofluorophotometer (RF-540, Shimadzu Ltd.) using 325 nm line of He–Cd laser as excitation source. All the measurements were taken at room temperature.

3. Results and discussion

Fig. 1 shows the SEM images of the electrospun ZnO nanofibers, and the insets are their corresponding enlarged images. Fig. 1(a) presents the typical morphologies of the as-spun undoped ZnO nanofibers before annealing. The randomly-oriented nanofibers with smooth surface and regular morphology show uniform diameter of about 150 nm and length up to several centimeters. After annealing in O_2 at 600 °C for 2 h, the obtained undoped and 5% Al-doped ZnO nanofibers remain a continuous nanostructure, as shown in Fig. 1(b) and (c), respectively. The surfaces of the nanofibers become rough and granular with grain size of 20-30 nm. Besides, compared with the grains of undoped ZnO nanofibers, the grains of 5% Al-doped ZnO nanofibers are much more loosely compacted.

Fig. 2 shows the XRD patterns of the Al-doped ZnO nanofibers with the Al concentration ranging from 0 to 5%. The observed peaks can be assigned to the (1 0 0), (0 0 2), and (1 0 1) etc. crystalline plane of hexagonal crystalline phase of ZnO materials (PDF# 361451). While no other XRD peaks corresponding to Al_2O_3 are detected in the Al-doped ZnO nanofibers. XRD analysis indicates that all the nanofibers are predominantly of polycrystalline hexagonal structure, in despite of the Al dopants. Further comparing the diffraction patterns of the undoped and doped samples, a shift to the large angle of diffraction peaks of 5% Al-doped ZnO compared with that of the undoped ZnO is observed, as shown in inset of Fig. 2. The shift of (1 0 0) and (0 0 2) peaks between the two samples were found to be 0.055° and 0.068°, respectively. The small shift could be attributed to the smaller atom radius of substituted Al^{3+} (0.53 Å) than that of Zn^{2+} (0.60 Å) in the polycrystalline lattice. The shift of the diffraction peaks indicates the incorporation of Al into the ZnO lattice. In addition, all samples exhibit broadened diffraction peaks.

Average diameters of the nanocrystallites of the samples were estimated from the most prominent three peaks of the XRD patterns by Scherrer formula, expressed as

$$d = \frac{0.89\lambda}{B\cos\theta}, \quad (1)$$

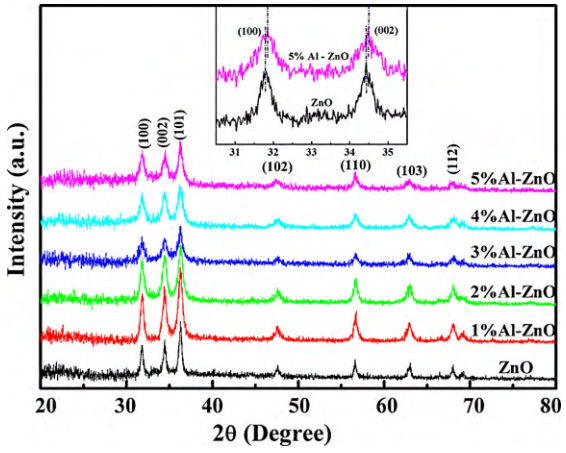

Fig. 2. XRD patterns of undoped and Al-doped ZnO with different concentration annealed at 600 °C in O_2, inset indicates the shift of the (1 0 0) and (0 0 2) peaks between undoped ZnO and 5% Al-doped ZnO.

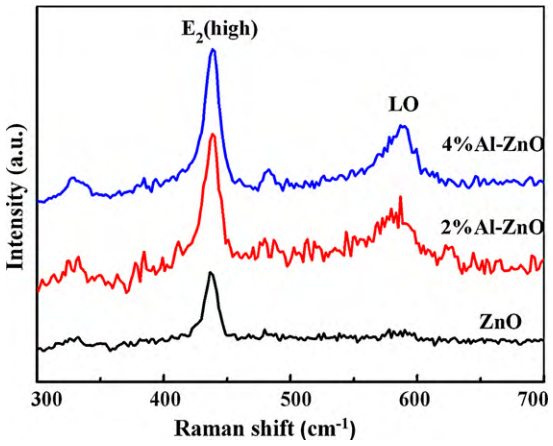

Fig. 3. Raman spectra of undoped and Al-doped ZnO with different concentration.

where d, λ, θ, and B are the mean grain size, the wavelength of X-ray, Bragg diffraction angle, and the full width at half maximum of the diffraction peak, respectively. It can be calculated that the average diameters of the nanofibers with Al doping concentration of 0–5% are 28.4, 19.3, 16.7, 17.4, 16.4 and 17.8 nm, respectively. Therefore, the incorporation of Al into ZnO could lead to the decrease of the grain size.

Fig. 3 shows the Raman spectra of the undoped and Al-doped ZnO (2% and 4%) annealed at 600 °C in O_2. All samples present an obvious band at 438 cm^{-1}, which can be assigned to E_2 (high) phonon scattering mode [26,27]. E_2 (high) mode, predominately associated with vibrations of O sublattice, is typical for ZnO hexagonal structure [26]. In addition, E_2 (high) mode is sensitive to the stress within the samples [28,29]. In this case, the peak shows no shift between undoped and Al-doped ZnO nanofibers. Thus the Al dopants did not introduce any additional stress into the samples. Besides, both Raman spectra of 2% and 4% Al-doped ZnO nanofibers present another vibration band at 587 cm^{-1}, which is contributions from both the A_1 (LO) and E_1 (LO) modes (LO scattering mode) due to random crystallite orientation [30]. Whereas, the LO mode can be barely seen from the undoped ZnO nanofibers. The enhancement of the LO mode by the Al doping has also been reported previously [27,31]. And it was attributed to the electric field induced (EFI) Raman scattering. The carrier concentration difference between the grain and the grain boundary leads to a depletion layer near the grain boundary, which further results in a built-in electric field within the separate grains. Since the intensity of the LO scattering is proportional to the electric field, and the strength of the electric field in the Al-doped grains is higher than that in the undoped grains because of the higher carrier concentration difference [27], Then the Al-doped ZnO nanofibers show an enhanced intensity of the EFI Raman scattering. Furthermore, according to the XRD data, grain size of Al-doped ZnO nanofibers decreased compared with that of undoped ZnO nanofibers. Thus, the higher density of grain boundary of Al-doped ZnO can also account for the enhancement of LO Raman scattering [30].

The PL spectra of the samples annealed in O_2 ambient at 600 °C with different Al doping concentrations (0%, 1%, 3%, and 5%) were shown in Fig. 4(a). It can be seen that the intensities of the NBE at 383 nm nearly keep the same for all the samples. However, the intensities of the broad luminescence bands in the visible range decrease dramatically with increasing Al doping concentration. When the Al content reaches 5%, the broad visible bands nearly disappear. The broad luminescence bands in the PL spectra of ZnO are believed to come from defects-related transitions [20,23]. However, the exact origins of the visible luminescence bands of ZnO are still not fully understood.

To investigate the origin of this phenomenon, the broad band in the PL spectrum of the undoped ZnO nanofibers was fitted into two peaks using a Gaussian profile, as shown in Fig. 4(b). The green and orange luminescence bands, locating at 533 and 620 nm show nearly the same intensity. The intensities of both luminescence bands decrease with increasing Al doping concentration.

As for the origin of the green luminescence band, there are mainly two hypotheses. One is the oxygen vacancy related radiative recombination [17,20]. The other is the surface defects-related recombination [32,33]. In our study, it can be found that the grain sizes decreased after Al doping, according to the XRD data, and the increased surface states related to the decreased intensity of green emission. Thus the green emission cannot be assigned to the surface defects. Then the green luminescence of the ZnO nanofibers might derive from the oxygen vacancies-related defects. To confirm above assumption, a control experiment has been conducted on between 4% Al-doped ZnO nanofibers annealed at 600 °C in air and O_2 atmosphere. The PL spectra of them are shown in Fig. 4(c). The intensity of the green band of the nanofibers annealed in O_2 is much lower that that of the sample annealed in air. This sharp contrast indicates that the green luminescence could be attributed to the oxygen vacancies, because the oxygen vacancies in the samples can be well compensated by the annealing treatments in the O_2 atmosphere.

On the other hand, the orange luminescence band of ZnO material has been less commonly observed compared with green luminescence band [18,19,21,23]. Mainly two mechanisms for the orange luminescence in ZnO have been proposed. One is associated with the excess oxygen [18,22,23], and the other is related to OH groups on the surface [24,25]. In our experiments, the annealing treatments in air or O_2 at high temperature could remove the OH groups from the samples thoroughly. This is to say that the origin of the orange luminescence could not be attributed to the OH groups. Furthermore, from Fig. 4(d), it can be seen that, compared with the undoped ZnO nanofibers annealed in O_2, the orange luminescence band of the undoped ZnO nanofibers annealed in air can be almost ignored, only one broad green luminescence centered at about 520 nm can be seen from the sample annealed in air. This contrast could prove that the orange luminescence is related to the excess oxygen.

From the above analysis, the green and orange luminescence bands could be attributed to the oxygen vacancies and excess oxygen, respectively. Similar phenomena have also been observed from the ZnO films, but with the green and yellow–orange luminescences competing with each other [11,22]. In addition, Wu et al. [21] have found that the green and orange luminescence bands were not observed simultaneously in ZnO nanorods. In our case, undoped ZnO nanofibers annealed in O_2 show both bands with nearly the same intensity (Fig. 4(b)), and Al-doping suppresses both luminescence bands. The reasonable explanation of the coexistence of the green and orange luminescences in ZnO nanofibers is that they come from different parts of the grains, which means that the oxygen vacancies and excess oxygen reside separately.

Furthermore, Zhong et al. [34] have reported that the defects acting as luminescence centers in ZnO ceramics localized in the vicinity of the grain boundaries rather than being distributed evenly throughout the grains. Here, basing on the PL data, it can be assumed that the oxygen vacancies should distribute inside the grains and the excess oxygen distribute near the grain boundaries. A schematic illustration of the distributions of both defects is presented in Fig. 5. The separate distribution can be attributed to the inward penetration of excess oxygen. For the undoped ZnO nanofibers annealed in air, the oxygen vacancies distribute evenly within the samples (Fig. 5(a)). However, after annealing in O_2, the oxygen vacancies near the grain boundaries could be compensated by O_2 in the atmosphere and the excess oxygen atoms would pen-

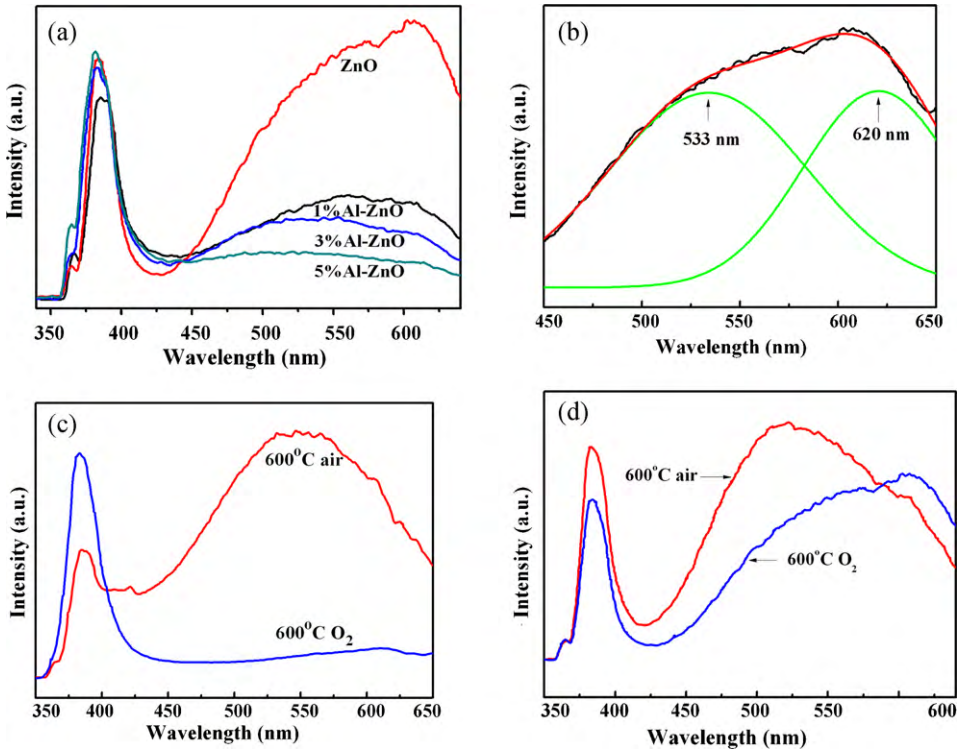

Fig. 4. (a) PL spectra of undoped and Al-doped ZnO with different concentration annealed at 600 °C in O_2. (b) Gauss fitting of PL spectra of undoped ZnO. (c) PL spectra of 4% Al-doped ZnO annealed at 600 °C in O_2 and air, respectively. (d) PL spectra of undoped ZnO annealed at 600 °C in O_2 and air, respectively.

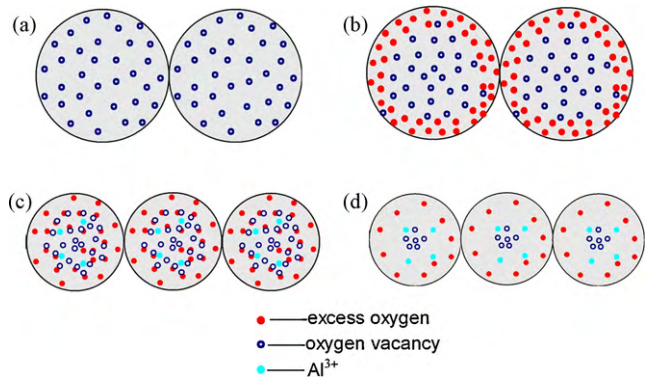

Fig. 5. Schematic illustrations of the distributions of oxygen vacancies and excess oxygen in undoped and Al-doped ZnO polycrystalline grains.

etrate inward the grains. Since the excess oxygen cannot penetrate too much in the undoped ZnO grains, the separation of oxygen vacancies and excess oxygen will form (Fig. 5(b)), which lead to the luminescence centers of green emissions inside the grains and that of orange emissions near the grain boundaries. For Al-doped ZnO, when Al substitutes Zn in the lattice, the diffusion depth of the excess oxygen will be larger than that of undoped ZnO due to the charge equilibrium (Fig. 5(c)). The penetrated excess oxygen will neutralize with the oxygen vacancies inside the grains. Thus both intensities of green and orange luminescences of Al-doped ZnO nanofibers decrease due to the decreased number of both luminescence centers (Fig. 5(d)). With increasing Al concentration in the ZnO nanofibers, the number of excess oxygen penetrating inward will increase, leading to the decreased intensities of luminescence bands. Moreover, in Al-doped ZnO nanofibers, the grain size decreases and the grains compact more loosely, compared with that of undoped ZnO nanofibers, making the excess oxygen and oxygen vacancies neutralize easily.

4. Conclusions

ZnO nanofibers doped with different Al concentration were fabricated by electrospinning method and subsequent annealing treatments. The nanofibers exhibited a typical ZnO hexagonal polycrystalline structure with diameter of about 150 nm. The size of polycrystalline grains of nanofibers decreased with the Al doping. PL spectra of all the samples presented two luminescence bands at green and orange ranges, and both decrease with increasing Al concentration. Analyses of the PL spectra of 4% Al-doped and -undoped ZnO nanofibers annealed in different atmosphere have indicated that the mechanisms of the green and orange luminescence bands are assigned to the oxygen vacancies and excess oxygen, respectively. A model has been proposed to illustrating the PL spectra. The oxygen vacancies residing inside the grains and the excess oxygen near the grain boundaries could account for the simultaneous decrease of both luminescence bands in the Al-doped ZnO nanofibers. From this research, it can be seen that the Al-doped ZnO nanofibers might be considered as one of the promising candidates of ultraviolet laser and light-emitting diodes material due to the suppression of Al doping on the defects luminescence of ZnO nanomaterials.

References

[1] L. Shi, Y.M. Xu, S.K. Hark, Y. Liu, S. Wang, L.M. Peng, K.W. Wong, Q. Li, Nano Lett. 7 (2007) 3559.
[2] Q. Wan, K. Yu, T.H. Wang, C.L. Lin, Appl. Phys. Lett. 83 (2003) 2253.
[3] L.E. Greene, M. Law, D.H. Tan, M. Montano, J. Goldberger, G. Somorjai, P.D. Yang, Nano Lett. 5 (2005) 1231.
[4] H.Z. Zhang, X.C. Sun, R.M. Wang, D.P. Yu, J. Cryst. Growth 269 (2004) 464.
[5] W.I. Park, G.-C. Yi, M. Kim, S.J. Pennycook, Adv. Mater. 14 (2002) 1841.
[6] C.-L. Cheng, J.-S. Lin, Y.-F. Chen, J. Alloys. Compd. 476 (2009) 903.
[7] X.M. Sui, C.L. Shao, Y.C. Liu, Appl. Phys. Lett. 87 (2005) 3.
[8] D.D. Lin, W. Pan, H. Wu, J. Am. Ceram. Soc. 90 (2007) 71.
[9] B. Zhou, Y.S. Wu, L.L. Wu, K. Zou, H.D. Gai, Physica E: Low Dimens. Syst. Nanostruct. 41 (2009) 705.
[10] S. Sasa, M. Ozaki, K. Koike, M. Yano, M. Inoue, Appl. Phys. Lett. 89 (2006) 053502.

[11] M. Wang, K.E. Lee, S.H. Hahn, E.J. Kim, S. Kim, J.S. Chung, E.W. Shin, C. Park, Mater. Lett. 61 (2007) 1118.
[12] H. Gong, J.Q. Hu, J.H. Wang, C.H. Ong, F.R. Zhu, Sens. Actuators B 115 (2006) 247.
[13] J.-P. Lin, J.-M. Wu, Appl. Phys. Lett. 92 (2008) 134103.
[14] X.L. Wu, G.G. Siu, C.L. Fu, H.C. Ong, Appl. Phys. Lett. 78 (2001) 2285.
[15] D. Li, Y.H. Leung, A.B. Djurisic, Z.T. Liu, M.H. Xie, S.L. Shi, S.J. Xu, W.K. Chan, Appl. Phys. Lett. 85 (2004) 1601.
[16] N.S. Norberg, D.R. Gamelin, J. Phys. Chem. B 109 (2005) 20810.
[17] K. Vanheusden, W.L. Warren, C.H. Seager, D.R. Tallant, J.A. Voigt, B.E. Gnade, J. Appl. Phys. 79 (1996) 7983.
[18] M.S. Wang, X.N. Cheng, J. Yang, Appl. Phys. A: Mater. Sci. Process. 96 (2009) 783.
[19] A.B. Djurisic, Y.H. Leung, K.H. Tam, L. Ding, W.K. Ge, H.Y. Chen, S. Gwo, Appl. Phys. Lett. 88 (2006) 103107.
[20] F.K. Shan, G.X. Liu, W.J. Lee, B.C. Shin, J. Appl. Phys. 101 (2007) 053106.
[21] L. Wu, Y. Wu, X. Pan, F. Kong, Opt. Mater. 28 (2006) 418.
[22] S.A. Studenikin, N. Golego, M. Cocivera, J. Appl. Phys. 84 (1998) 2287.
[23] J.W.P. Hsu, D.R. Tallant, R.L. Simpson, N.A. Missert, R.G. Copeland, Appl. Phys. Lett. 88 (2006) 252103.
[24] A.B. Djurisic, Y.H. Leung, K.H. Tam, Y.F. Hsu, L. Ding, W.K. Ge, Y.C. Zhong, K.S. Wong, W.K. Chan, H.L. Tam, K.W. Cheah, W.M. Kwok, D.L. Phillips, Nanotechnology 18 (2007) 095702.
[25] S. Li, X.Z. Zhang, B. Yan, T. Yu, Nanotechnology 20 (2009) 495604.
[26] R. Jothilakshmi, V. Ramakrishnan, R. Thangavel, J. Kumar, A. Sarua, M. Kuball, J. Raman Spectrosc. 40 (2009) 556.
[27] M. Tzolov, N. Tzenov, D. Dimova-Malinovska, M. Kalitzova, C. Pizzuto, G. Vitali, G. Zollo, I. Ivanov, Thin Solid Films 379 (2000) 28.
[28] A.J. Cheng, Y.H. Tzeng, H. Xu, S. Alur, Y.Q. Wang, M. Park, T.H. Wu, C. Shannon, D.J. Kim, D. Wang, J. Appl. Phys. 105 (2009) 073104.
[29] J.N. Zeng, J.K. Low, Z.M. Ren, T. Liew, Y.F. Lu, Appl. Surf. Sci. 197–198 (2002) 362.
[30] C. Roy, S. Byrne, E. McGlynn, J.P. Mosnier, E. de Posada, D. O'Mahony, J.G. Lunney, M.O. Henry, B. Ryan, A.A. Cafolla, Thin Solid Films 436 (2003) 273.
[31] H.W. Kim, M.A. Kebede, H.S. Kim, Curr. Appl. Phys. 10 (2010) 60.
[32] I. Shalish, H. Temkin, V. Narayanamurti, Phys. Rev. B 69 (2004) 245401.
[33] H.M. Zhong, Q. Liu, Y. Sun, W. Lu, Chin. Phys. B 18 (2009) 5024.
[34] J. Zhong, A.H. Kitai, P. Mascher, W. Puff, J. Electrochem. Soc. 140 (1993) 3644.